# Quantitative Measurement of Viscoelastic Properties of Soft Membranes Subjected to Finite Deformations Based on Optical Coherence Elastography

**O. Balogun and Z. Wang**

**Abstract** Glaucoma is a leading cause of irreversible blindness that affects over 60 million people worldwide. Glaucomatous eyes are associated with risk factors such as elevated intraocular pressure (IOP) and low corneal hysteresis. Reliable non-invasive measurement of IOP remains a formidable challenge that limits the accurate diagnosis of glaucoma and associated intervention therapies. This work investigates the propagation of shear-dominated elastic waves in hydrostatically inflated corneal tissue phantoms based on the optical coherence elastography (OCE) technique. Unlike previous approaches reported in the literature, we analyze the dispersion relation of guided elastic waves in the phantoms by accounting for both small amplitude viscoelastic wave propagation and finite static deformations. The analytical approach we adopted will enable the determination of the storage and loss shear moduli dependence on finite strains in the cornea that results from hydrostatic pressures. This work provides a modeling and experimental framework for accurately characterizing viscoelastic properties and the IOP of corneal tissues.

**Keywords** OCE · Shear wave propagation · Hyper-viscoelasticity

## Introduction

Glaucomas are a group of optic neuropathies that lead to vision loss and blindness [1]. Elevated intraocular pressure (IOP) is a significant risk factor for the development of glaucoma, and IOP reduction is the only treatment shown to be effective in stopping or slowing the disease progression [2–11]. Recent studies have shown that current clinical methods for the measurements of the IOP can be inaccurate in some patients [11–14] and lead to erroneously low or high IOP measurements. Currently utilized measurement techniques do not account for variations in the corneal structure and biomechanical properties. Thus, there is an unmet clinical need for improved methods to accurately measure the IOP and to account for the intrinsic variability of the cornea biomechanical properties.

Corneal tissue is a complex, layered material that exhibits elastic, viscous, and anisotropic deformation in response to mechanical stimuli. The cornea is subjected to a biaxial tensile stress state at elevated IOP levels due to fluid loading from the anterior chamber. The resulting cornea deformation depends on its five-layered microstructure, the stroma being the dominant layer. Recently, the optical coherence tomography (OCT) technique emerged as a powerful technique routinely used in ophthalmology practice to characterize cornea tissue morphology with micron-scale lateral spatial resolution. Integrating dynamic mechanical stimuli with the OCT allows for local excitation, detection of elastic waves [15], and measurement of cornea tissue elastic properties. The latter approach is commonly called the optical coherence elastography (OCE) technique. Recently, the OCE technique was used to characterize the IOP-dependent elastic wave speeds and the anisotropic shear stiffness constants in porcine corneal tissue [16, 17]. However, while these measurements are promising for OCT/OCE diagnosis of glaucomas, they ignore the influence of large static deformations of the cornea that occur at elevated IOP levels. The large deformation can significantly modulate the viscoelastic properties due to the realignment of collagen fibrils in the

O. Balogun (✉)
Department of Mechanical Engineering, Northwestern University, Evanston, IL, USA

Department of Civil and Environmental Engineering, Northwestern University, Evanston, IL, USA
e-mail: o-balogun@northwestern.edu

Z. Wang
Department of Civil and Environmental Engineering, Northwestern University, Evanston, IL, USA



C. Franck et al. (eds.), *Challenges in Mechanics of Biological Systems and Materials, Thermomechanics and Infrared Imaging, Time Dependent Materials and Residual Stress, Volume 2*, Conference Proceedings of the Society for Experimental Mechanics Series,
https://doi.org/10.1007/978-3-031-50470-9_3

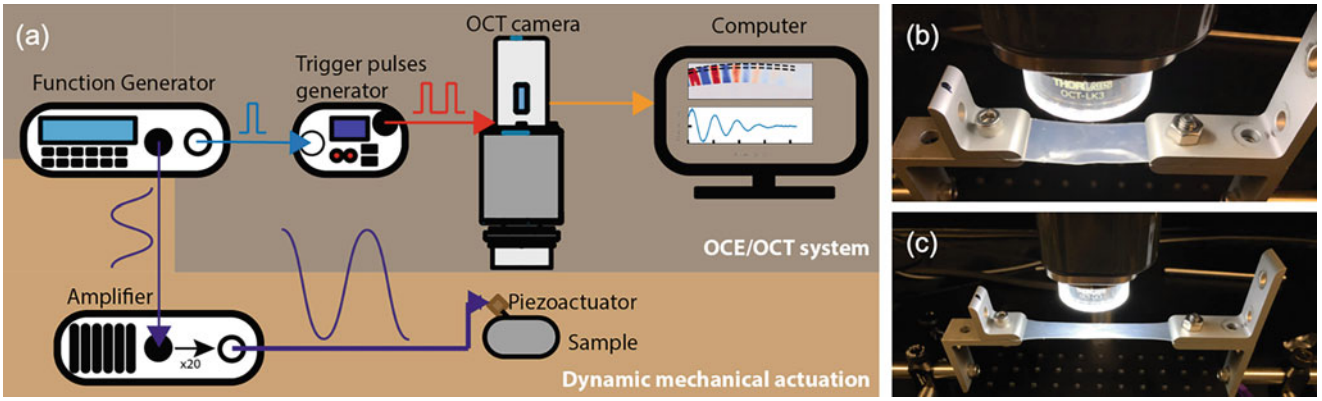


**Fig. 1** Experimental setup with the optical coherence elastography/tomography (OCE/OCT) system and the dynamic mechanical actuation system. (**a**) The thin rubber membrane sample is mounted on the uniaxial stretch device under the OCT camera. The stretch ratio ($\lambda_1$) of the rubber sample is controlled by a precision translation stage between (**b**) $\lambda_1 = 1.0$ and (**c**) $\lambda_1 = 1.9$

stroma. To address this deficiency, first, we begin with a study of the influence of finite tensile deformation on the viscoelastic properties of a thin silicon rubber membrane subjected to uniaxial tension. Silicon rubber provides a surrogate model for the cornea tissue that eliminates the complexity associated with the anisotropic properties of corneal and the biaxial tensile state resulting from hydrostatic membrane loading. We can also study the biaxial tensile loading of the silicone membrane with an inflated membrane geometry. In this paper, we characterize the shear storage and loss moduli based on OCE measurements of the guided elastic wave velocity and attenuation in the rubber membrane. By applying uniaxial stretches between 1 and 1.9, we observe a corresponding modulation in the elastic wave speeds and wave amplitude decay, reflecting the membrane's stretch-dependent viscoelastic properties. We also explore a hyper-viscoelasticity framework for inverse analysis of the stretch-dependent elastic wave speed and attenuation to estimate the storage and loss moduli based on OCE measurements.

## Background

In this section, we present a brief description of the OCT and OCE approaches and some experimental measurements in a silicone rubber membrane. Figure 1a shows a schematic illustration of the OCT/OCE experimental setup. The OCT microscope (Thorlabs GAN210C1, NJ, USA) is a low-coherence interferometer that transduces local variations in the morphology or displacement to optical intensity or phase signals. Elastic waves are generated by a paddle actuator and detected by the OCT interferometer. The actuator consists of a knife edge that is attached to the tip of a resonant piezoelectric (PZT) transducer (PA4CEW, Thorlabs) at one end. The other end of the knife edge is placed in contact with the sample surface. An amplified sinusoidal voltage from a function generator is used to drive the PZT transducer, leading to the local oscillatory tapping motion of the sample. Harmonic elastic waves generated in the sample by the oscillatory indentation of the sample propagate away from the actuation point, leading to local dynamic displacement in the sample. The OCT interferometer tracks the local out-of-plane displacement of the sample. Further details of the OCT/OCE approaches are available in our previous papers [18, 19]. In this work, we study the propagation of elastic waves in a thin silicone rubber membrane subjected to uniaxial tension. The polymer was made from EcoFlex 00-10 following the description in Royston et al. [20] The sample is mounted on a uniaxial stretching device and placed under the OCT camera, as shown in Fig. 1b, c.

## Analysis

Figure 2a shows a two-dimensional OCT structural image of the sample for a stretch ratio of 1.0. The grayscale image corresponds to the backscattered intensity of the probe light, varying from black at the minimum level to white at the maximum. Two bright lines in the image occur at the top and bottom boundaries due to the large refractive index mismatch between the membrane and the surrounding air. The few dark vertical stripes within the sample are due to tiny air bubbles in the sample. The OCT image is uniform, suggesting that the sample is homogeneous. Figure 2b shows the corresponding OCE

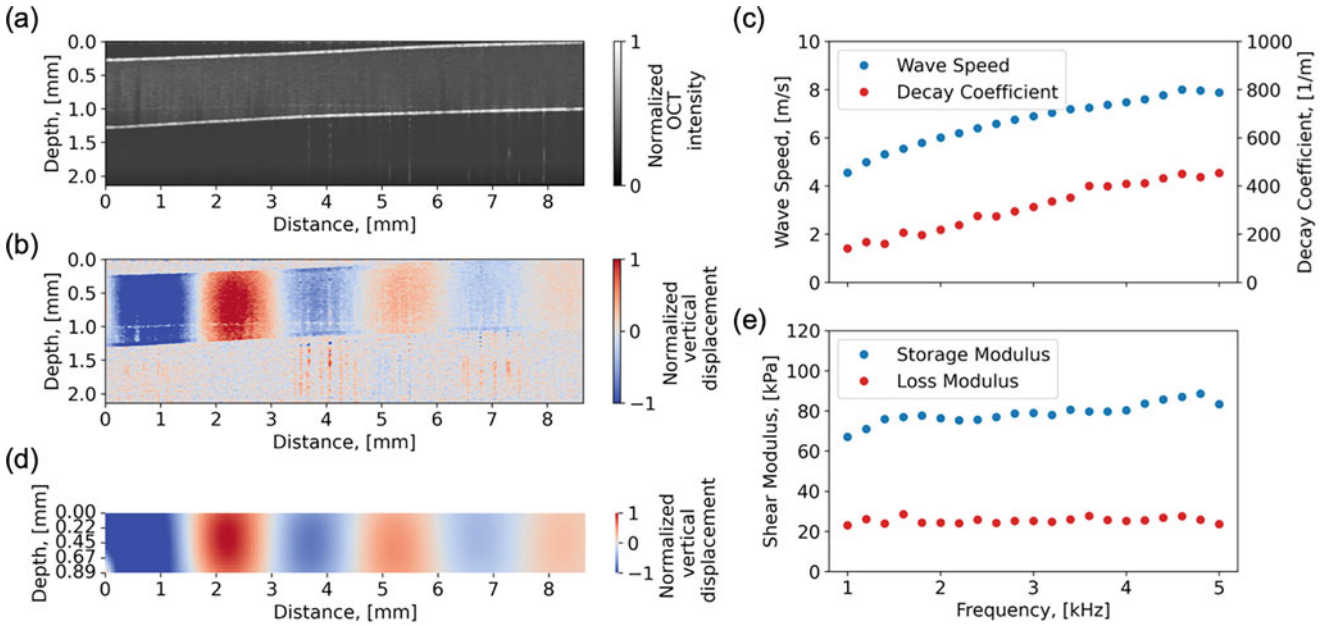


**Fig. 2** Experimental results from the rubber membrane. (**a**) OCT image of the rubber membrane. (**b**) OCE image of the rubber membrane at 2 kHz. (**c**) The rubber membrane's wave speeds and decay coefficients from 1 to 5 kHz. (**d**) Numerically calculated vertical displacement field in the membrane for a harmonic excitation frequency of 2 kHz. (**e**) Estimated storage moduli and loss shear moduli for the rubber membrane

image. For the measurement, the PZT transducer was excited with a 2 kHz sinusoidal voltage. The periodic red-blue fringes in the image represent the spatial variation of the optical phase difference between the backscattered light and a reference light beam in the OCT interferometer. The phase difference is proportional to the local vertical displacement and refractive index [15]. The red-blue contrast in the image is due to the variation of the vertical displacement from positive (or upward moving) to negative (or downward moving) values. The local vertical displacement field is uniform through the depth of the sample. However, the displacement varies periodically in the lateral direction with a nearly constant wavelength. Additionally, the displacement decreases with distance from the excitation source. Similar behaviors are observed for excitation frequencies between 1 and 5 kHz, indicating that elastic waves within this range are attenuated with propagation distance due to a combination of material damping and diffraction.

To extract the wavelength and amplitude decay coefficient in the measured OCE data, first, we averaged multiple line scans from different depths in the OCE image to obtain a single displacement waveform. An exponentially decaying sinusoidal function, $I(t) = Ae^{-\alpha(f)x} \times \sin(2\pi x/\lambda(\mathrm{f}) - \theta)$, is fitted to the resulting displacement waveform, where $c(\mathrm{f}) = \lambda(\mathrm{f}) \times \mathrm{f}$ is the elastic wave speed, $\lambda(\mathrm{f})$ is the wavelength, and f is the elastic wave frequency. $\lambda(\mathrm{f})$ is equal to the spatial period of the fringe pattern in the OCE image, and $\theta$ is a phase constant. $(f)$ is the amplitude decay coefficient $\alpha(f)$. To eliminate the effects of diffraction on $\alpha$, we applied a diffraction correction factor to displacement waveform following the description in Ruiz and Nagy [21], since the width of the knife edge actuator (3 mm) is smaller than the longest propagation distance (i.e., ~ 9 mm) for the measured displacement field for the elastic waves in the membrane. The diffraction correction eliminates the displacement amplitude decay that stems from purely geometric effects like the finite size of the excitation source. Figure 2c shows the wave speeds and decay coefficients obtained from the displacement profiles for 1 to 5 kHz frequencies. The wave speed increases with frequency, going from 4.5 m/s at 1 kHz to 7.9 m/s at 5 kHz. The frequency-dependent wave speed (i.e., the phase velocity dispersion curve) is consistent with the theoretical dispersion curve for the membrane's zeroth-order $A_0$ antisymmetric Lamb wave mode in a thin plate [22]. Unlike Lamb waves in an elastic plate, the decay coefficient for the guided waves in the silicone membrane increases with the frequency from 140 to 450 $\mathrm{m}^{-1}$, suggesting that the elastic wave dissipation increases with frequency.

We estimate the sample's frequency-dependent shear storage and loss moduli by fitting a visco-elastodynamic model for an incompressible thin silicone membrane to the measured elastic wave speed and amplitude decay coefficient. The thickness of the sample is estimated from the OCT image in Fig. 1a. The sample density is assumed to be 965 $\mathrm{kg/m}^3$ [20]. Figure 2d shows the calculated displacement field in the membrane produced with a 2 kHz harmonic normal surface line load. The wavelength and amplitude decay ratio for displacement fields matches the diffraction-corrected experimental data. Figure 2e shows the best-fit frequency-dependent storage and loss shear moduli. Between 1 and 5 kHz, the shear storage modulus increases from 67 to 88 kPa. On the other hand, the shear loss modulus remains nearly constant and close to 25 kPa. The measured viscoelastic properties are being validated against low frequency shear rheometry measurements.

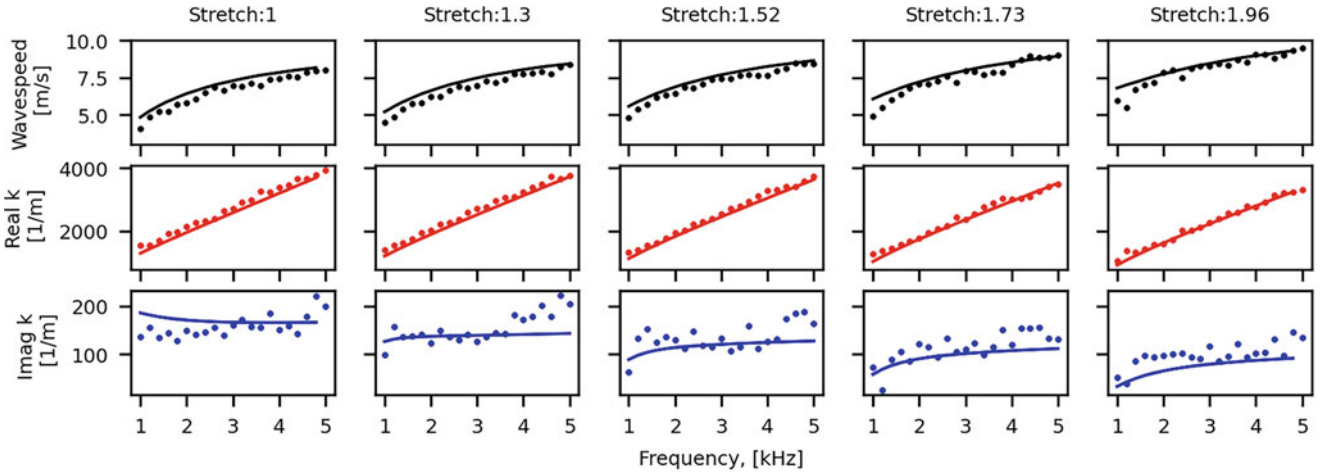


**Fig. 3** OCE measurements (dots) and hyper-viscoelastic model (lines) of elastic wave speeds, real and imaginary components of the wavenumbers of guided waves in a silicone rubber membrane subjected to uniaxial stretch ratios from 1 to 1.96

Figure 3 shows the wave speeds and real and imaginary components of the wavenumbers for stretch ratios between 1 and 1.9. The real part of the wavenumber ($k^{'}$) is related to the wavelength ($\lambda$) by $k^{'} = 2\pi/\lambda$, while the imaginary part of the wavenumber ($k^{''}$) is the damping coefficient $\alpha$. With an increasing stretch ratio, the wave speed increases, while the damping coefficient decreases. These results suggest that the material gets stiffer and less viscous with increasing uniaxial static deformation. To evaluate the membrane's stretch-dependent storage and loss modulus, we adopt the two-potential constitutive relation for rubber viscoelasticity developed by Kumar and Lopez-Paimes [23]. We employ the constitutive relation in the incremental equilibrium equations of motion [24] to calculate the frequency-dependent wave speed and amplitude decay for incremental guided wave motion that is superimposed on the finite deformation of the membrane. The preliminary numerical predictions from the model (solid line in Fig. 3) and the OCE measurements (dotted lines) are in good agreement, albeit that the goodness of the fits needs to be improved. The best-fit material properties, i.e., the stretch-dependent shear storage and loss moduli, will be reported in a later publication. Upon improving the quality of the data fitting, the modeling framework will be extended to investigate a hydrostatically loaded membrane in a state of biaxial tension and to simulate the effect of the hydrostatic pressure on the viscoelastic properties.

## Conclusion

This work presents an experimental approach for viscoelastic characterization of soft membranes subjected to finite static deformations. Specifically, the experimental approach relies on measuring the frequency-dependent wave speed and amplitude decay coefficient for guided elastic waves in the membrane at different uniaxial stretch ratios. The preliminary results obtained for stretch ratios between 1 and 1.9 suggest that increasing the stretch ratio makes the membrane stiffer and less viscous. We incorporated a hyper-viscoelastic constitutive model for the stretched membrane into the elastodynamic equations to calculate the wave speed and amplitude decay coefficient of guided waves in the membrane. By matching these results to the measured data, we can estimate the stretch-dependent viscoelastic properties of the membrane. The proposed method can be used to study and characterize the viscoelastic behavior of soft membrane materials subjected to finite static deformations. In the future, we will explore the modeling and experimental approach to characterize the IOP dependence of the viscoelastic properties of corneal tissues.

## References

1. Weinreb, R.N., Aung, T., Medeiros, F.A.: The pathophysiology and treatment of glaucoma: a review. JAMA. **311**(18), 1901–1911 (2014)
2. Robert, S.: A history of intraocular pressure and its measurement. Optom. Vis. Sci. **88**(1), E16–E28 (2011)
3. Mark, H.H.: Armand Imbert, Adolf Fick, and their tonometry law. Eye. **26**(1), 13–16 (2012)
4. Wessels, I.F., Oh, Y.: Tonometer utilization, accuracy, and calibration under field conditions. Arch. Ophthalmol. **108**, 1709–1712 (1990)

5. van der Jagt, L.H., Jansonius, N.M.: Three portable tonometers, the TGDc-01, the ICARE and the Tonopen XL, compared with each other and with Goldmann applanation tonometry*. Ophthalmic Physiol. Opt. **25**, 429–435 (2005)
6. Deol, M., Taylor, D.A., Radcliffe, N.M.: Corneal hysteresis and its relevance to glaucoma. Curr. Opin. Opthalmol. **26**(2), 96–102 (2015)
7. Susanna, C.N., Diniz-Filho, A., Daga, F.B., Susanna, B.N., Zhu, F., Ogata, N.G., Medeiros, F.A.: A prospective longitudinal study to investigate corneal hysteresis as a risk factor for predicting development of glaucoma. Am J. Ophthalmol. **187**, 148–152 (2018)
8. Liu, J., Roberts, C.J.: Influence of corneal biomechanical properties on intraocular pressure measurements: quantitative analysis. J. Cataract Refract. Surg. **31**, 146–155 (2005)
9. Guarnieri, F.A.: Corneal biomechanics. In: Corneal Biomechanics and Refractive Surgery, pp. 7–31. Springer, New York (2015)
10. Kohlhaas, M., Boehm, A.G., Spoerl, E., Pursten, A., Grein, H.J., Pillunat, L.E.: Effect of central corneal thickness, corneal curvature, and axial length on applanation tonometry. Arch. Opthalmol. **124**, 471–476 (2006)
11. Killer, H.E., Pircher, A.: Normal-tension glaucoma: review of current understanding and mechanisms of the pathogenesis. Eye (Lond.). **32**(5), 924–930 (2018)
12. Heijl, A., Leske, M.C., Bengtsson, B., Hyman, L., Bengtsson, B., Hussein, M., Early Manifest Glaucoma Trial Group: Reduction of intraocular pressure and glaucoma progression: results from the Early Manifest Glaucoma Trial. Arch. Ophthalmol. **120**(10), 1268–1279 (2002)
13. Anderson, D.R., Drance, S.M., Schulzer, M., Collaborative Normal-Tension Glaucoma Study Group: Factors that predict the benefit of lowering intraocular pressure in normal-tension glaucoma. Am J. Ophthalmol. **136**(5), 820–829 (2003)
14. Wolfs, R.C., Klaver, C.C., Vingerling, J.R., Grobbee, D.E., Hofman, A., de Jong, P.T.: Distribution of central corneal thickness and its association with intraocular pressure: the Rotterdam Study. Am J. Ophthalmol. **123**(6), 767–772 (1997)
15. Kirby, M.A., Pelivanov, I., Song, S., Ambrozinski, L., Yoon, S.J., Gao, L., Li, D., Shen, T.T., Wang, R.K., O'Donnell, M.: Optical coherence elastography in opthalmology. J. Biomed. Opt. **22**(12), 1–28 (2017)
16. Ambrozinski, L., Song, S., Yoon, S.J., Pelivanov, I., Li, D., Gao, L., Shen, T.T., Wang, R.K., O'Donnell, M.: Acoustic micro-tapping for non-contact 4D imaging of tissue elasticity. Sci. Rep. **6**, 1–11, 38967 (2016)
17. Pitre, Jr. J.J., Kirby, M.A., Li, D.S., Shen, T.T., Wang, R.K., O'Donnell, M., Pelivanov, I.: Nearly-incompressible transverse isotropy (NITI) of cornea elasticity: model and experiments with acoustic micro-tapping OCE. Sci. Rep. **10**, 1–14, 12983 (2020)
18. Liou, H.C., Sabba, F., Packman, A.I., Wells, G., Balogun, O.: Nondestructive characterization of soft materials and biofilms by measurement of guided elastic wave propagation using optical coherence elastography. Soft Matter. **15**, 575–585 (2019)
19. Liou, H.C., Sabba, F., Packman, A.I., Rosenthal, A., Wells, G., Balogun, O.: Towards mechanical characterization of granular biofilms by optical coherence elastography measurement of circumferential elastic waves. Soft Matter. **15**, 5562–5573 (2019)
20. Royston, T.J., Dai, Z., Chaunsali, R., Liu, Y., Peng, Y.: Estimating material viscoelastic properties based on surface wave measurements: a comparison of techniques and modeling assumptions. J. Acoust. Soc. Am. **1130**, 4126–4138 (2011)
21. Ruiz, M.A., Nagy, P.B.: Diffraction correction for precision surface acoustic wave velocity measurements. J. Acoust. Soc. Am. **112**, 835–842 (2002)
22. Simonetti, F.: Lamb wave propagation in elastic plates coated with viscoelastic materials. J. Acoust. Soc. Am. **115**, 2041–2053 (2004)
23. Kumar, A., Lopez-Pamies, O.: On the two-potential constitutive modeling of rubber viscoelastic materials. Comptes Rendus Mecanique. **344**, 102–112 (2016)
24. Ogden, R.W.: Incremental statics and dynamics of pre-stressed elastic materials. In: Waves in Nonlinear Pre-stressed Materials, pp. 1–26. Springer, Vienna (2007)